Coarse graining of *NN* inelastic interactions up to 3 GeV: Repulsive versus structural core

P. Fernández-Soler[1,*] and E. Ruiz Arriola[2,†]

[1]*Instituto de Física Corpuscular (IFIC), Centro Mixto CSIC-Universidad de Valencia, Institutos de Investigación de Paterna, Apartado 22085, E-46071 Valencia, Spain*

[2]*Departamento de Física Atómica, Molecular y Nuclear and Instituto Carlos I de Física Teórica y Computacional Universidad de Granada, E-18071 Granada, Spain*

The repulsive short-distance core is one of the main paradigms of nuclear physics which even seems confirmed by QCD lattice calculations. On the other hand nuclear potentials at short distances are motivated by high energy behavior where inelasticities play an important role. We analyze *NN* interactions up to 3 GeV in terms of simple coarse grained complex and energy dependent interactions. We discuss two possible and conflicting scenarios which share the common feature of a vanishing wave function at the core location in the particular case of *S* waves. We find that the optical potential with a repulsive core exhibits a strong energy dependence whereas the optical potential with the structural core is characterized by a rather adiabatic energy dependence which allows one to treat inelasticity perturbatively. We discuss the possible implications for nuclear structure calculations of both alternatives.

I. INTRODUCTION

The nuclear hard core was postulated by Jastrow in 1951 [1], based on the observation that *pp* scattering presents a flat and almost angle independent differential cross section at about 100–200 MeV, a feature that he found to be easily reproduced by a hard sphere of radius $a_c = 0.6$ fm. This finding has been corroborated by more complete analyses reaching larger energies. Actually, in his analysis above 1 GeV in 1958, Brown found that the core remained below this energy but made the intriguing claim "The hard core is assumed to disappear with increasing energy and to be replaced by absorption" [2]. The repulsive core has become one of the well accepted paradigms of nuclear physics, providing a possible explanation for nuclear stability for high density states. Also, the short-distance properties are relevant for neutron matter in the core of a neutron star with a Fermi momentum about twice that of nuclear matter, $k_F \sim 600$ MeV, and hence a corresponding reduced wavelength $1/k_F \sim 0.3$ fm. The nuclear physics evidence [3] for this prominent feature is shown to be the zero crossing of the $^1S_0$ *NN* phase shift at $T_{\text{LAB}} \sim 300$ MeV, right after the opening of the pion production threshold. In line with these early developments, the Hamada-Johnston potential became the archetype of a hard core potential with a common core radius $a_c = 0.5$ fm [4], and the Reid potential confirmed these findings with both a hard core and a soft core type structure [5,6] (see also [7] for a comprehensive review).

That was much of the discussion in those days in nuclear physics, with the core having a visible effect in the nuclear and neutron matter equations of state [8]. A readable historical account can be found in Ref. [9]. The usual characterization of the hard core requires the use of local (or weakly nonlocal) potentials. Indeed, the Argonne potential saga befits this viewpoint [10–12] and is the natural evolution of these developments allowing benchmarking calculations in nuclear

structure of light nuclei (for reviews see, e.g., Refs. [13,14] and references therein).

In this paper we want to analyze critically the evidence of the nuclear core, which ultimately proves crucial for nuclear structure and nuclear reactions calculations at intermediate and high energies. We do so by paying attention to the scattering process at those energies probing the core size.

In order to motivate our analysis below it is pertinent to review several aspects and features of the nuclear core within various contexts. This is done in Sec. II, where we review some of the history on the repulsive and structural cores and their corresponding fingerprints. We also discuss critically aspects of the problem based on recent lattice QCD results, as well as the more phenomenological approaches which demand a realistic treatment of relativity, inelasticity, and spin degrees of freedom. An analysis of the relevant scales in the problem is undertaken in Sec. III, trying to be as pedagogical as possible. There we show that the largest laboratory energies at which a partial wave analysis (PWA) has been carried out in the past actually probe the region where the core sets in, but do not resolve the fine structure of the core shape. In Sec. IV we present some numerical results revisiting aspects of the coarse graining idea in the elastic case for fits up to 300 MeV and 1 GeV. Full consideration of inelasticities is undertaken in Sec. V, in which we extend the idea to the case of an optical potential and provide fits up to 3 GeV, where we confront two validated and conflicting scenarios: the repulsive core and the structural core. In Sec. VI we provide some discussion and outlook for future work. Finally, in Sec. VII we summarize our results and main conclusions.

II. THE NUCLEAR SHORT DISTANCE CORE

A. Early origins of repulsive and structural core

The origin of the repulsive core has been the subject of many investigations. Within the one-boson exchange (OBE) picture where nucleons exchange all possible mesons $\pi, \eta, \sigma, \rho, \omega, \ldots,$

*pedro.fernandez@ific.uv.es
†earriola@ugr.es

the repulsive core has traditionally been attributed to the ω-meson exchange by Nambu [15] and many others [16], but with an unnatural coupling $g_{\omega NN} \sim 20$ [9] even in the extremely successful CD-Bonn potential [17] which largely violates SU(3) expectations, $g_{\omega NN} = 3g_{\rho NN} \sim 10$, and would represent a unrealistically large deviation (about 50%) from this symmetry.[1] A relativistic origin of the core was prompted by Gross [19].

An alternative origin of the repulsive core, the so-called structural core [7,20,21] was proposed many years ago and is based on the composite nature of the nucleon and the Pauli principle at the constituent level, which implies that the zero energy wave function has a zero at the core radius but does not vanish below it. This implies the existence of forbidden deeply bound states [22], a fact accommodated naturally by quark cluster models [23] that has motivated the series of Moscow potentials [24]. The connection with forbidden states in the light of high energy scattering data below 6 GeV was addressed in Ref. [25]. A readable and fresh account of these well documented short-range components of nuclear forces can be found in a recent paper by Kukulin and Platonova [26]. It is noteworthy that within the OBE picture it has been found that, if an SU(3)-natural coupling $g_{\omega NN} = 3g_{\rho NN} \sim 10$ is assumed, the ω-exchange repulsion is overcome by attractive ρ and σ exchanges triggering a net short-distance strong attraction, and a spurious deeply bound state in the $^1S_0$ channel is generated. As a consequence of the oscillation theorem, the corresponding wave function at zero energy develops a node which is located at about the standard and traditionally accepted core position [27].

B. The nuclear core from QCD

The ultimate answer on the existence of the core and its properties should come from QCD. In fact, recent QCD lattice calculations claim to find a repulsive core at about similar distances in the quenched approximation [28,29]. This is done by placing two heavy sources made of three quark fields with nucleon quantum numbers at the same point, $J_N(x) \sim q(x)q(x)q(x)$, located at a given fixed separation $\vec{r}$, and studying the propagation of the corresponding correlators for long enough Euclidean times, providing the corresponding static energy $E_{NN}(r) \sim 2M_N + V_{NN}(r)$. Moreover, an application of the operator product expansion provides an understanding of short-distance $V_{NN}(r) \sim 1/(M_N r^2)$ type repulsions among pointlike baryons in QCD [30].

On general grounds one should expect pion production when $V_{NN}(r_\pi) \gtrsim m_\pi$, in which case the potential should develop an imaginary part as the system becomes unstable against the decay $NN \to NN\pi$ and pions will eventually be radiated. This feature is precluded in the quenched approximation where particle creation is suppressed. Alternatively one could, in addition to just NN states, implement $NN\pi$ configurations [for instance taking $J_\pi(x) \sim \bar{q}(x)\vec{\tau}\gamma_5 q(x)$ located at $x = 0$], still within the quenched approximation, in
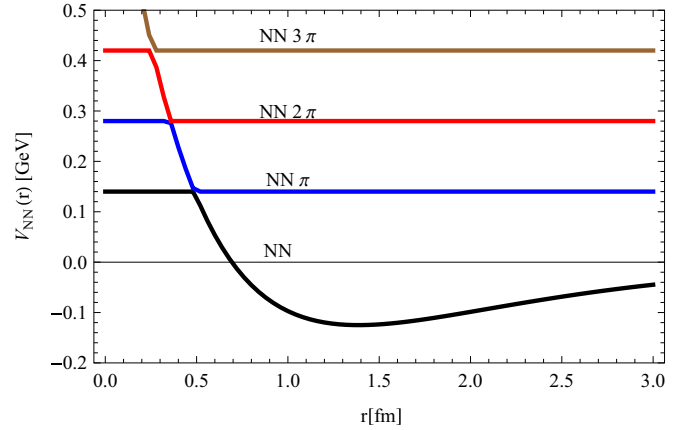

FIG. 1. Phenomenon of avoided crossing expected from a lattice calculation of the static NN energy as a function of the distance, $E_{NN}(r) = 2M_N + V_{NN}(r)$, in the Hilbert space spanned by NN and multipion states, $\mathcal{H} = \mathcal{H}_{NN} \oplus \mathcal{H}_{NN\pi} \oplus \mathcal{H}_{NN2\pi} \oplus \dots$. Anytime a crossing with a $n\pi$ threshold occurs, $V_{NN}(r_n) = nm_\pi$, the system chooses the minimum energy state with the pions at rest. The potential $V_{NN}(r)$ with the repulsive core corresponds to the envelope of all the different branches.

which case one has a coupled channel Hamiltonian spanning the trial Hilbert space, $\mathcal{H} = \mathcal{H}_{NN} \oplus \mathcal{H}_{NN\pi}$, and incorporating, besides $NN \to NN$ and $NN\pi \to NN\pi$ diagonal elements, the $NN \to NN\pi$ transition. Schematically, one has

$$\mathcal{H}(r) - 2M_N = \begin{pmatrix} V_{NN,NN}(r) & V_{NN,NN\pi}(r) \\ V_{NN,NN\pi}(r) & m_\pi + V_{NN\pi,NN\pi}(r) \end{pmatrix}. \quad (1)$$

The eigenvalues of this Hamiltonian may be denoted by $E_-(r) < E_+(r)$ and clearly one has the variational relation $E_-(r) \leqslant V_{NN,NN}(r) + 2M_N$. Under these circumstances, an avoided crossing pattern, familiar from molecular physics in the Born-Oppenheimer approximation [31] will occur as a function of the separation distance r, choosing the lower energy $NN\pi$ branch below the pion-production distances. The situation is sketched in Fig. 1 for the case of avoided crossings with several pions, assuming a small channel mixing and vanishing $V_{NN,n\pi;NN,n\pi}(r)$ for simplicity.

Of course, this argument can be generalized when further inelastic channels, such as $N\Delta$ or $\Delta\Delta$, are open. From a variational point of view, we always have

$$\min E_n(r) \leqslant V_{NN,NN}(r) + 2M_N, \quad (2)$$

so that we can regard the repulsive core found in QCD lattice calculations [28,29] as an upper bound of the true static energy within the restricted two nucleon Hilbert space, $\mathcal{H}_{NN}$, and *not* as a genuine feature of the NN interaction. This observation is one of our main motivations for the present paper.

C. High energy NN analysis

While the discussion of the core shape and details had some impact in nuclear matter and the nuclear equation of state, one can also undertake a similar analysis more directly within a free nucleon scattering context. Definitely, a hard or soft repulsive core located at a short distance such as $a_c = 0.5$ fm

---

[1] For the role played by 2π exchange as a scalar meson see, e.g., Ref. [18] and references therein.

can only be resolved and isolated from the rest of the potential when the relative de Broglie reduced wavelength becomes of much smaller size, i.e., $1/p_{\text{CM}} \ll a_c$. This means going up to laboratory energies $T_{\text{LAB}} = 2p_{\text{CM}}^2/M_N \gg 340$ MeV, above pion production threshold and well beyond the traditional domain of *NN* potentials used in nuclear physics for nuclear structure and nuclear reactions. Fortunately, there exist by now abundant data of *pp* and *np* scattering, permitting a model independent partial wave analysis going up to $T_{\text{LAB}}^{\text{max}} = 3$ GeV [32], i.e., $p_{\text{CM}}^{\text{max}} = 1.2$ GeV, allowing a direct reconstruction of scattering amplitudes [33–35] from complete sets of experiments. In general, phase shifts can only be considered observables when a complete set of measurements (differential cross sections, polarization asymmetries, etc.) for a fixed energy has been made. In the late 1970s and until today extensive fits have been undertaken in the region below the onset of diffractive scattering. The *NN* PWA at energies well above the pion production threshold also has a long history, and a good example of subsequent upgrades is represented by the series of works conducted by Arndt and collaborators [36–41] (see also the GWU database [42]). The most recent GWU fit [43] is based on a parametrization [37] with a total number of 147 parameters, and fitting up to a maximum of all $J = 7$ partial wave amplitudes (phases and inelasticities) up to 3 GeV deals with a large body of 25 362 *pp* data (with $\chi^2 = 48\,780.934$) and 13 033 *np* data (with $\chi^2 = 26\,261.000$), which is sufficient for our considerations here.

D. Short-distance correlations

In many respects the short-distance aspects of the *NN* interaction are relevant for nuclear physics at intermediate energies. The typical example is provided by short-distance correlations, where the traditionally accepted repulsive core should become more visible. Experimentally, such effects might be "seen" in two-nucleon knock out experiments (e, e', NN) and they would be responsible for the high-momentum pair distribution [44]. Large scale calculations generate such distributions using a real *NN* potential to solve the nuclear many body problem [45–48]. Of course, at relative center-of-mass (CM) momenta where $p = \sqrt{M\Delta} \sim 2k_F \sim 600$ MeV and $\Delta = M_\Delta - M_N = 0.297$ GeV (the Δ-N splitting), the inelasticity becomes large and the interaction in free space cannot be fixed by a real and energy independent *NN* potential. This corresponds to back-to-back collisions of particles on the surface of the Fermi sphere and provides a natural cutoff for these momentum distributions stemming from real *NN* potentials. In a recent study [49] this issue has been analyzed, and it has been found that for CM momenta below $p \lesssim \sqrt{M\Delta}$ ($T_{\text{LAB}} \lesssim 2\Delta$) there is no need for a nuclear repulsive core. In fact, the main contribution stems from the midrange attractive part. In scattering experiments, particles are on-shell and that means that energy and momentum are related. In finite nuclei, where particles are off-shell, we can witness short-distance properties, i.e., high momentum states, keeping their energy inside the nucleus small. Therefore, that means that an energy independent *NN* interaction might be fixed directly from the high-momentum distribution rather than from *NN* scattering. In any case, the traditional evidence of the repulsive core

based on short-distance correlations should be revised when inelasticities are taken into account.

E. Relativity and inelasticity

In *NN* scattering at the high energies under consideration, $T_{\text{LAB}} \lesssim 3$ GeV we have three essential features: spin degrees of freedom, opening of inelastic channels, and relativity. At these energies, and since $\sqrt{s} \sim 2M_N + nm_\pi$, up to a maximum eight pions (among other things) can be produced. The full multichannel calculation directly embodying $NN \rightarrow NN + n\pi$ transitions is prohibitive and has never been carried out. In reality many fewer pions are produced, on average $\bar{n} \sim 2$, since the largest contributions to the inelastic cross section stem from resonance production and decay, say $NN \rightarrow N\Delta \rightarrow NN\pi$ or $NN \rightarrow 2\Delta \rightarrow NN2\pi$, etc., triggered by peripheral pion exchange.

The general field theoretical approach would require a coupled channel Bethe-Salpeter equation, where the kernel would ultimately be determined phenomenologically from the *NN* scattering data (see, e.g., [50]). Under these circumstances the effort of solving the Bethe-Salpeter equation may be sidestepped by a much simpler procedure, namely the invariant mass framework [51], which corresponds to solving

$$\mathcal{M}^2 \Psi \equiv 4\left(-\nabla^2 + M_N^2\right)\Psi + M_N V \Psi = s \Psi, \qquad (3)$$

with s the standard Mandelstam variable, and to identifying the relativistic and nonrelativistic CM momenta $p_{\text{CM}}^2 = s/4 - M_N^2$ yielding an equivalent Schrödinger equation with a potential V. We will incorporate inelastic absorption via an optical (complex) potential,

$$V(r, s) = \text{Re } V(r, s) + i \text{ Im } V(r, s), \qquad (4)$$

by appealing to the standard Feshbach justification [52,53] of separating the Hilbert space into elastic and inelastic sectors corresponding to the P and Q orthogonal projectors. Field theoretical approaches assuming the conjectured double spectral representation of the Mandelstam type provide a link to this optical potential as well as its analytic properties in the s variable [54,55]. Optical potential approaches have already been proposed in the past in this energy range, and an early implementation of the optical potential in *NN* scattering within the partial wave expansion was carried out in Ref. [56]. A more microscopic description involves explicitly $N\Delta$ inelastic channels (see, e.g., Ref. [50] and references therein). A relativistic complex multirank separable potential of the neutron-proton system was proposed in Ref. [57,58]. The approach we use here furnishing both relativity and inelasticity has already been exploited in the much higher energy range covering from the CERN Intersecting Storage Rings (ISR) up to the Large Hadron Collider (LHC), $\sqrt{s} = 25$–7000 GeV [59,60].

In this paper we will approach the problem by suitably adapting the coarse graining idea presented in a series of papers to this new inelastic situation [61–66]. As already mentioned, at the partial waves level most of the evidence about the core comes from the S waves, so we will restrict our study to this simple case.

III. SHORT-WAVELENGTH FLUCTUATIONS

A. Inverse scattering

In order to motivate our subsequent discussion, let us approach the problem from an inverse scattering point of view (for a review see, e.g., [67]). Such inverse scattering methods have also been extended within *NN* scattering in the inelastic regime [68,69], and to some extent represent a model independent determination of the underlying interaction. By all means these approaches require a complete description of the phase shift from threshold up to infinity, i.e., $0 < p_{CM} < \infty$. In practice, any truncation at high energies, say $p_{CM} = \Lambda$, generates a short-wavelength ambiguity $\Delta r = \hbar/\Lambda$ which we can regard as a short-distance fluctuation, since finer resolutions will effectively become physically irrelevant. This should not be a problem for a real potential where only elastic scattering may take place, and since Levinson's theorem guarantees the phase-shift to go to zero at high energies. For a complex potential where inelastic channels are open, the situation may be quite different in practice, since, first, we do not have a Levinson's theorem and, second, the optical potential may not even go to zero at high energies[2]

Inverse scattering methods also allow a geometric glimpse into the *NN* inelastic hole at several distances and energies [70,71] when a repulsive core is assumed for laboratory energies below 3 GeV, although it has also been recognized that this solution is not unique [69]. In the case of Ref. [72], where relativistic optical potentials on the basis of the Moscow potential and lower phase shifts for nucleon scattering at laboratory energies up to 3 GeV were considered, it was found that there was no core representation of the inverted interaction for energies above 1 GeV. Actually, in Ref. [73] one can identify the oscillations of the resulting local potential. These short-wavelength fluctuations/oscillations are inherent to the maximum energy or CM momentum Λ being fixed for the phase shift. The local projection method based on closely related ideas also produces very similar oscillations [74].

B. Coarse graining

Under these circumstances we will invoke from a Wilsonian point of view the coarse graining of the interaction down to the shortest resolution scale in the problem. This is based on the reasonable expectation that wavelength fluctuations shorter than the smallest de Broglie wavelength, which determine the maximal resolution given by $\Delta r \sim 1/p$, are unobservable. For a potential $V(r)$ with a typical range r_c this simply means taking a grid of points which is chosen for convenience to be equidistant, $r_n = n\Delta r$, and using the potential at the grid points $V(r_n) = V_n$ as the fitting parameters themselves. On the other hand, the long-range part of the potential will be taken to

be given by one-pion exchange (OPE) above $r_c = 3$ fm,[3] thus we will have

$$V(r) = V_{\text{Short}}(r)\theta(r_c - r) + V_{\text{OPE}}(r)\theta(r - r_c), \qquad (5)$$

where in the $^1S_0$ *pn* channel

$$V_{\text{OPE}}^{^1S_0}(r) = -3f^2 \frac{e^{-m_\pi r}}{r}. \qquad (6)$$

Of course, there are many possible ways to coarse grain the inner component of the interaction $V_{\text{Short}}(r)$ and a particularly simple one has been to take a sum of delta shells as initially proposed by Avilés in 1973 [75] and reanalyzed in Ref. [61] (see [62,63,65] for pedagogical reviews) and pursued in latter studies [66] (a comprehensive mathematical analysis can be consulted in Ref. [76]) yielding the most accurate determination of $f^2 = 0.0763(1)$ [77] when charged pions and many other effects are considered. Here, we will not attempt this very high accuracy and take the more conventional values $f^2 = 0.075$ and $m_\pi = 140$ MeV for simplicity. In this paper, we will take also a piecewise square-well (SW) potential for definiteness and, because it looks more intuitive, will use it for the main presentation. Of course, none of our main results depends on the particular regularization and we will provide also results for the delta-shell (DS) coarse graining. Our notation will be as follows:

$$V_{\text{GR}}^I(r) = V_{\text{SW}}(r) \equiv \sum_{i=1}^{N} V_i^{\text{SW}} \theta(r_{i-1} < r \leqslant r_i), \qquad (7)$$

$$V_{\text{GR}}^{II}(r) = V_{\text{DS}}(r) \equiv \sum_{i=1}^{N} \Delta r\, V_i^{\text{DS}} \delta(r - r_i), \qquad (8)$$

$$r_n = n\Delta r. \qquad (9)$$

Note that roughly we expect $V_i^{\text{SW}} \approx V_i^{\text{DS}}$. The corresponding *S*-wave Schrödinger equation has to be solved with the boundary conditions

$$u(0) = 0, \quad u(r) \to \sin[pr + \delta(p)]. \qquad (10)$$

From the continuity of the function and the (dis)continuity of the derivative it is then straightforward to obtain a recurrence relation whence the total accumulated phase shift may be obtained. The approximations involved in Eqs. (7) and (8) can be regarded as simple integration methods for the Schrödinger equation; i.e., given a potential $V(r)$ we can take grid points $r_n = n\Delta r$ and $V_n \equiv V(r_n)$. We obviously expect that, at the *fine* graining limit, i.e. $\Delta r \to 0$ and $N \to \infty$ with $r_c = N\Delta r$ fixed, we get an arbitrarily good solution to the wave function. We give below the corresponding discretized formulas for the two cases.

---

[2]For instance, in Ref. [50] the modeling of nucleon-nucleon scattering above 1 GeV has been addressed, signaling a gradual failure of the traditional one boson exchange (OBE) picture, which needs rescaling by $1/s$ of the OBE potential.

[3]The choice of this boundary is not arbitrary; it has been motivated from comprehensive PWA at energies around pion production threshold (see below).

1. Square well

For a sequence of square well potentials $U_1, \ldots, U_N$ with $U_i \equiv 2\mu V(r_i)$, the solution can be written piecewise:

$$u_0(r) = \sin(K_1 r + \delta_0), \quad 0 < r < r_1, \tag{11}$$

$$u_1(r) = \sin(K_2 r + \delta_1), \quad r_1 < r < r_2, \tag{12}$$

$$\vdots \tag{13}$$

$$u_N(r) = \sin(K_{N+1} r + \delta_N), \quad r_N < r, \tag{14}$$

where $K_n = \sqrt{-U_n + k^2}$. We take $\delta_0 = 0$, and δ_n is the accumulated phase shift due the sequence of square wells, so that $\delta(k) = \delta_N(k)$. Matching the logarithmic derivative at every r_i, we get the recursion relation

$$\cot \delta_{n+1} = \frac{A_n + B_n \cot \delta_n}{C_n + D_n \cot \delta_n}, \tag{15}$$

where

$$A_n = K_{n+1} \cot(K_n r_n) - K_n \cot(K_{n+1} r_n), \tag{16}$$

$$B_n = K_n \cot(K_n r_n) \cot(K_{n+1} r_n) + K_{n+1}, \tag{17}$$

$$C_n = K_{n+1} \cot(K_n r_n) \cot(K_{n+1} r_n) + K_n, \tag{18}$$

$$D_n = K_{n+1} \cot(K_{n+1} r_n) - K_n \cot(K_n r_n). \tag{19}$$

2. Delta shells

For the sequence of delta-shell potentials with coefficients $\Delta r U_1, \ldots, \Delta r U_N$, the solution can similarly be written piecewise:

$$u_0(r) = \sin(kr + \delta_0), \quad 0 < r < r_1, \tag{20}$$

$$u_1(r) = \sin(kr + \delta_1), \quad r_1 < r < r_2, \tag{21}$$

$$\vdots \tag{22}$$

$$u_N(r) = \sin(kr + \delta_N), \quad r_N < r. \tag{23}$$

As before, we take $\delta_0 = 0$, and δ_n is the accumulated phase shift due the sequence of square wells. Matching the logarithmic derivative at any r_n, we get the recursion relation

$$k \cot(kr_n + \delta_{n+1}) - k \cot(kr_n + \delta_n) = U_n \Delta r. \tag{24}$$

C. Counting parameters for the optical potential

In contrast to a conventional integration method, where the integration step Δr is an auxiliary parameter which should be removed as $\Delta r \to 0$ based on the accuracy of the wave function, in the coarse graining approach $\Delta r \sim 1/p_{\mathrm{CM}}$ becomes a physical parameter which only goes to zero when the scattering energy goes to infinity, and the precision is dictated by the experimentally measurable phase shifts. One of the advantages of this point of view is that we avoid using specific functional forms which possibly correlate different points in the potential and hence introduce a bias in the analysis. A crucial question is to know how many *independent* fitting parameters $V(r_n)$ are needed to produce a good fit to the scattering data going to a maximum CM momentum p. The

simple answer for the S wave is just $N \sim r_c / \Delta r = p r_c$. (for higher partial waves and coupled channels see, e.g., [65]).[4]

This very simple idea underlies comprehensive benchmarking *NN* studies about pion production threshold undertaking a complete PWA [61–63,65,66]. In this work we will extend, to the case of interest, the idea of complex optical potentials where the imaginary component of the potential takes care of the absorption. Definitely, for this analysis to be competitive, the number of parameters must be controllable *a priori*. The coarse graining involves also the inelasticity hole, which we assume to be of the order of the traditional nuclear core, as will be verified below. Therefore, in our analysis in S waves and up to the highest energies, we consider the inelasticity as pointlike since $\Delta r \sim a_c$, an assumption which will be justified below.

Resolving the core structure in more detail requires going to higher energies, where there is no PWA, so that the separate contribution of the S wave could be analyzed. Therefore, either more complete data will be needed or other methods can be used. For instance, above 3 GeV Regge behavior sets in and we refer to recent works undertaking such an analysis [78,79]. At much higher energies such as those measured at ISR ($\sqrt{s} \sim 25$–50 GeV) and LHC ($\sqrt{s} \sim 2000$–14000 GeV) and sufficiently large momentum transfers, one has $\Delta r \ll a_c$ and the structure of the inelasticity hole can be pinned down more accurately, assuming spin independent interactions [59,60].

IV. ELASTIC COARSE GRAINING REVISITED

In previous works by the Granada group [64] extensive use of delta-shell based coarse graining potentials has been made in order to carry out the most comprehensive *NN* fit to date up to 350 MeV. This was done for a total of $N_{\mathrm{Dat}} = 6713\ np + pp$ scattering observables slightly above the pion production threshold with a very high statistical quality, $\chi^2/\nu = 1.04$, and a total number of $N_{\mathrm{Par}} = 46$ independent parameters, providing some confidence in the method. In this section we revisit the fit for the $^1S_0$ channel by using instead a piecewise square-well potential. As already said, and in harmony with previous findings, we will assume OPE interaction above $r_c = 3$ fm.

A. Fit to 300 MeV

Let us consider for definiteness the Gaussian-OPE potential obtained in Ref. [80] in the $^1S_0$ channel, which as we see from Fig. 2 presents a repulsive core starting at 0.6 fm. We may integrate the differential equation by using any standard procedure, such as Numerov's method (see, e.g., Ref. [81] and references therein) where the precision is on the determination of the wave function as a primary quantity. In order to

---

[4]If one disregards the OPE tail above $r_c = 3$ fm, the delta-shell method provides in momentum space [61] a multirank separable potential very much in the spirit of the proposal in Refs. [57,58]. Our coarse grain argument does in fact foresee *a priori* the rank of the interaction; it coincides with the number of grid points N. This result holds also when the inelasticity is taken into account (see below).
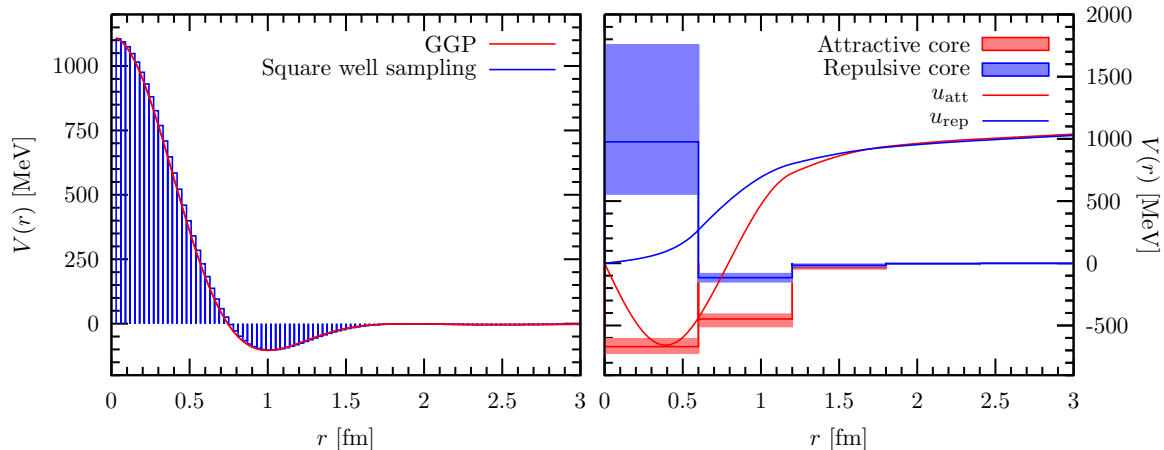
FIG. 2. Left panel: Granada smooth Gaussian potential in the $^1S_0$ channel [80] and the sequence of square wells with heights V_n sampling the values of the original potential $V_n \equiv V(r_n)$. The total number of points is $N = 40$. Right panel: (Short distance) Attractive and repulsive coarse grained sequence of square wells fitted to the Granada phase shifts up to 300 MeV laboratory energy. Uncertainties stem from the phase shifts. The total number of points is $N = 4$. We also plot the corresponding zero energy wave function in arbitrary units.

reproduce the phases with the smallest uncertainty quoted in Ref. [80] and taking a maximum integration distance of $R = 5$ fm, we need $M = 2^{14} = 16\,384$ integration points. For our purposes this high pointwise accuracy in the wave function is not strictly necessary, as the wave function is not an observable, and we are merely interested in determining the physically measurable phase shift.

Therefore, we may regard the piecewise solutions described in Sec. III B as integration methods and study the accuracy with respect to the phase shift and *not* with respect to the wave function. For instance, if we use a piecewise square well potential as an integration method using Eq. (15), we get that about 40 wells [whose values are given by the potential $U_i = U(r_i)$] prove sufficient, a result shown in Fig. 2. This corresponds to the *fine graining* point of view for a *prescribed* potential.

However, the potential was obtained from a fit to data, and in this case to the phase shift. The question now is how many *fitting* wells, $U_1^{\text{Fit}}, \ldots, U_N^{\text{Fit}}$, separated by Δr are needed to reproduce the same phase shift to a certain accuracy up to a maximal energy value, which we take here to be 300 MeV. As already anticipated, the answer is $N = 5$, a much smaller value

than with the fine graining case. Our results are again shown in Fig. 2 and as we see there are two possible solutions, corresponding to *attractive* and *repulsive* potentials. We will refer to them as A and R respectively and the numerical values can be looked up in Table I. For completeness the delta-shell fitting values are also presented in Table II. The existence of two solutions in itself is not surprising as it reflects and illustrates in the coarse grained framework the well-known ambiguities of the inverse scattering problem [68]. The physical reason is that the corresponding wavelength does not sample the short-distance region with sufficient resolution. As a matter of fact we will see that these two solutions depart from each other at energies higher than those used in the fitting procedure.

B. Fit to 1 GeV

It is natural to think that by increasing the energy we will be able to resolve more accurately the short-distance region. More specifically, we might be able to pin down the nature of the nuclear core as well as better discriminating between both solutions A and R found before and eventually ruling out one or both solutions. As said, above pion production threshold the potential must reflect the inelasticity, but we also expect this effect to be located at short distances as suggested by the small inelastic cross section. Therefore, in a first attempt we will take $T_{\text{LAB}} < 1$ GeV and fit just the real part of the phase shift with a real and energy independent potential.

TABLE I. Values of the squared well potentials at the given sampling points obtained fitting up to $T_{\text{LAB}} = 300$ MeV for both the attractive (A) and repulsive (R) solutions. They are obtained from a fit to a number of $N_d = 10$ data with a corresponding $\chi^2 = 2.9$. The central values and uncertainties of the parameters were obtained as expected values and standard deviations from set of fits to synthetic data, generated from the experimental uncertainties.

r_i (fm)	V_i^{SW}(MeV) - A	V_i^{SW}(MeV) - R
0.6	−661(48)	1175(536)
1.2	−459(43)	−119(30)
1.8	−35(8)	−16(9)
2.4	−5(1)	−3(3)
3.0	−0.1(0.4)	−0.4(0.8)

TABLE II. Same as Table I but for delta shells.

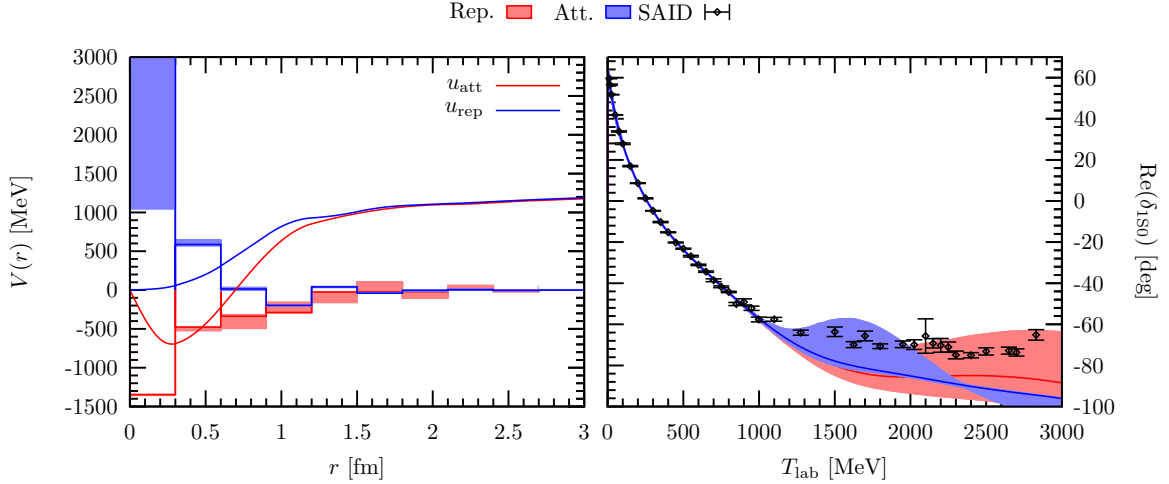| r_i (fm)	V_i^{DS} (MeV) - A	V_i^{DS} (MeV) - R
0.6	−265(4)	127(20)
1.2	−293(6)	−66(5)
1.8	−64(7)	−3(3)
2.4	−2(2)	−3(2)
3.0	−2(4)	1(3)

FIG. 3. Left panel: (Short distance) Attractive and repulsive coarse grained sequence of square wells fitted to the real part of the SAID $^1S_0$ *np* phase shifts up to 1 GeV laboratory energy. Uncertainties stem from the phase shifts. The total number of points is $N = 10$. We also plot the corresponding zero energy wave function in arbitrary units. Right panel: Comparison of the fits with the SAID database up to 3 GeV.

In our analysis at higher energies we will profit from the PWA carried out by several groups in the past and will use the GWU database [42] for definiteness. Moreover, we will restrict ourselves to the simplest case of the most important *S* waves since our main purpose is to merely show that the coarse graining works at much higher energies also when inelasticities are included. In fact, *S* waves have the smallest possible impact parameter $b = 1/(2p)$ sensing the core region. In a further publication we will extend the analysis to higher partial waves.

Let us briefly review the basic idea and count the number of necessary parameters. The maximum resolution corresponds to the shortest de Broglie wavelength, which is $\lambda = 0.3$ fm. On the other hand, we assume, as in the low energy analysis, that from $r_c \geqslant 3$ fm the only contribution is due to one pion exchange. Thus, we have to sample $r_c/\Delta r = 10$ points.

The result of the fit is now presented in Fig. 3. We get $\chi^2/\nu = 1.6$ in both cases, which shows that inelasticity must be taken into account even if only the real part of the phase shift is fitted (see below). By all means, when we are dealing with a real potential where the inelasticity is small but nonzero, we may wonder what is the uncertainty in the potential associated

to this. Numerical values with their uncertainties for the repulsive and attractive cores in the SW and DS approaches can be seen in Tables III and IV respectively.

C. Quality of fits

The quality of fits can be tested in a number of ways, including the χ^2 test (see, e.g., [82]). The verification of these tests ensures uncertainty propagation. For completeness, we also show in Table V the moments test for the lowest moments, and as we see the test validates error propagation within the expected fluctuations due to a finite number of fitting data. In all quoted results the central values and uncertainties of the parameters were obtained as expectation values and standard deviations from set of fits to synthetic data, generated from the experimental uncertainties using the bootstrap method [83].

D. Evolution of potentials as a function of the fitting energy

In order to illustrate the coarse graining idea, we show in Fig. 4 the evolution of the phases as the maximal fitting energy is gradually increased in the repulsive core case. Essentially

TABLE III. Same as Table I but fitting up to $T_{LAB} = 1000$ MeV. In this case $\chi^2 = 33.9$ and $N_d = 24$.

r_i (fm)	V_i^{SW}(MeV) - A	V_i^{SW}(MeV) - R
0.3	$-1352(34)$	6851(1553)
0.6	$-494(28)$	360(285)
0.9	$-395(84)$	66(64)
1.2	$-234(72)$	$-195(6)$
1.5	$-81(70)$	17(29)
1.8	32(66)	$-11(31)$
2.1	$-56(42)$	$-26(23)$
2.4	32(25)	17(14)
2.7	$-13(10)$	$-8(7)$
3.0	2(3)	0(2)

TABLE IV. Same as Table III but considering delta shells. The chi-squared value obtained in this case is $\chi^2 = 33.0$.

r_i (fm)	V_i^{DS} (MeV) - A	V_i^{DS} (MeV) - R
0.3	$-741(20)$	4643(2000)
0.6	$-430(111)$	533(97)
0.9	$-377(21)$	$-233(20)$
1.2	$-143(4)$	$-4(10)$
1.5	$-25(3)$	$-34(5)$
1.8	$-13(6)$	$-6(5)$
2.1	$-13(4)$	$-8(4)$
2.4	11(3)	6(4)
2.7	$-7(2)$	$-5(3)$
3.0	3(3)	1(3)

TABLE V. Test of the normality of the residuals relative to the fits involving delta shells and square wells. Note that the different moments μ_r must be compared with the standard gaussian distribution $\mathcal{N}(0,1)$ moments in the last column.

| | $T_{\text{LAB}}^{\max} = 0.3$ GeV | | | | $T_{\text{LAB}}^{\max} = 1$ GeV | | | | $\mathcal{N}(0,1)$ |
	SW - A	SW - R	DS - A	DS - R	SW - A	SW - R	DS - A	DS - R	
μ_3	−0.37	−0.18	−0.08	−0.07	−0.11	−0.11	−0.17	−0.15	0 ± 1.223
μ_4	2.65	2.63	2.47	2.53	2.89	2.89	2.87	2.89	3 ± 3.093
μ_5	−2.89	−1.64	−0.87	−0.79	−1.24	−1.24	−1.61	−1.50	0 ± 9.681
μ_6	9.83	9.23	8.12	8.49	11.5	11.5	11.4	11.5	15 ± 31.827
μ_7	−15.0	−8.53	−4.46	−4.11	−8.80	−8.80	−10.7	−10.2	0 ± 115.842
μ_8	39.6	34.1	28.0	29.6	50.6	50.6	50.4	50.8	105 ± 434.016

we just take as a guide that $\Delta r \sim 1/p_{\text{CM,max}}$ and the number of square wells is approximately given by $N \sim r_c/\Delta r$. The errors are propagated from the fitting results beyond the fitting range. As we see, already with $N = 5$ the prediction band contains the scattering analysis interactive dial-up (SAID) data for which we plot both the real and imaginary parts of the phase shift. A close study of the evolution of the phases was carried out in a previous work [49] taking the AV18 potential [12] as a reference interaction, which reproduces *a fortiori* the scattering data. There the coarse graining of the interaction with delta shells was studied with similar conclusions. Here, besides using the square wells we also analyze the impact of phase-shift uncertainties stemming from the fits to the experimental data in the analysis. The evolution of the square well potentials as a function of the maximal fitting energy together with the corresponding wave function with the shortest wavelength are depicted in Fig. 5, illustrating the meaning of coarse graining in this particular case.

V. COARSE GRAINED OPTICAL POTENTIALS

We come now to the fit up to 3 GeV, which, as mentioned above, is the largest laboratory energy where a complete PWA
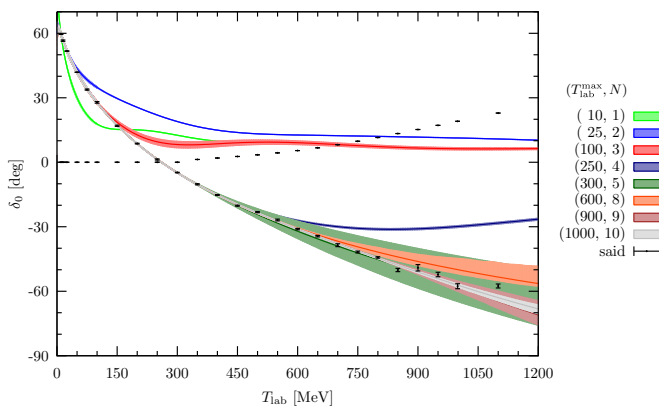

FIG. 4. *np* phase shifts (in degrees) in the $^1S_0$ channel as a function of the LAB energy (in MeV). We show gradual fits in the repulsive core case to increasingly high energies to the real part of the phase-shift with an increasing number of square wells with the corresponding extrapolated errorbands. For illustration we also show the imaginary part of the phase shift (non-fitted).

has been undertaken and hence the particularly interesting $^1S_0$ wave has been extracted. Of course, at these high energies one may produce up to seven pions among other particles, a circumstance that is beyond any comprehensive theoretical analysis at present due to the large number of coupled channels and multiparticles states. Therefore, and in line with previous developments and the discussion above, we will use an optical potential. At the energies where the inelastic cross section is sizeable, relativistic corrections start playing a role. As mentioned above we will implement relativity by invoking the invariant mass framework [51] and as already exploited in recent high energy studies [59].

In general the coarse grained optical potential will be complex, and a pertinent question is, what is the range of the inelasticity? We address this issue by noting that the inelastic cross section jumps from $\sigma_{\text{in}} = 1$ mb to $\sigma_{\text{in}} = 28$–32 mb in the CM range $\sqrt{s} = 2.3$–2.7 GeV [84] (for a review see, e.g., [32] and references therein), which corresponds to nucleon resonance excitations $NN \to N\Delta$ or $NN \to \Delta\Delta$ for $M_N + M_\Delta \lesssim \sqrt{s} \lesssim 2M_\Delta$, i.e., $\sqrt{M\Delta} \lesssim p \lesssim \sqrt{2M\Delta}$ with $\Delta = M_\Delta - M_N$, and remains almost constant ± 1 mb up to 1000 GeV. We show as an illustration σ_{in} in Fig. 6 up to 3 GeV laboratory energy. In the energy range we are concerned with $\sigma_{\text{in}} \sim \sigma_{\text{el}}$ so that the absorbing black disk picture holds. That means that the size of the hole is about 1 fm. There are at least two ways to represent the absorptive S matrix: either as a complex phase-shift or as a real phase-shift and an inelasticity. The relation between them is

$$S_l(p) = \eta_l(p)e^{2i\delta_l(p)} = e^{-2\rho_l(p)}e^{2i\delta_l(p)}. \quad (25)$$

On the other hand, the inelastic cross section can be written as a sum over partial waves,

$$\sigma_{\text{in}} = \frac{\pi}{p^2} \sum_{l=0}^{\infty} (2l+1)[1 - \eta_l(p)^2]. \quad (26)$$

In the impact parameter representation where we can set $(l + 1/2) = bp$, the S wave involves the shortest impact parameter $b_{\min} = 1/(2p) = 1/\sqrt{s - 4M^2}$, and at this level we can see from Fig. 7 that, $1 - \eta_0(p)^2$ vanishes for b larger than the coarse graining scale $\Delta r = 0.3$ fm. Thus, we will assume *just one* complex and energy dependent fitting parameter for the innermost potential well, i.e., at $r = r_1 \equiv \Delta r$,

$$V(r_1, p) = \text{Re } V(r_1, p) + i \text{ Im } V(r_1, p) \equiv \text{Re } V_1 + i \text{ Im } V_1, \quad (27)$$
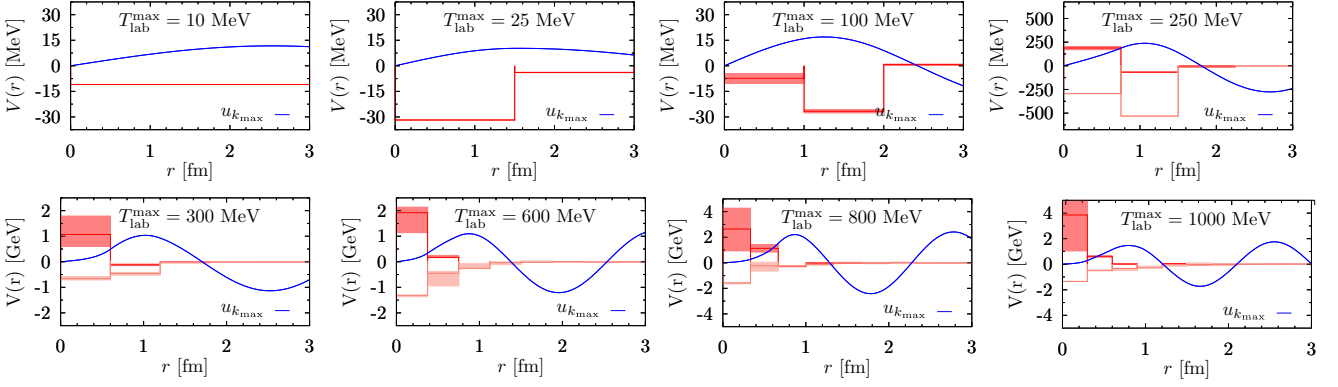
FIG. 5. The evolution of the different square well potentials with the maximal fitting laboratory energy. For illustration we also plot the maximum energy wave function in arbitrary units. The bifurcation between the repulsive and attractive core cases occurs at about 250 MeV.

and keep the remaining $N - 1$ points fixed and energy independent to the values of the previous fit at $T_{\mathrm{LAB}} = 1$ GeV. The previous recursion relations, Eq. (15), hold also here by just replacing $\delta_l(p) \rightarrow \delta_l(p) + i\rho_l(p)$. The inelasticity and energy dependence at $r = r_1$ already improves the previous fit from $\chi^2/\nu = 1.6$ to $\chi^2/\nu = 0.7$.

Our procedure is as follows: for any energy value we fit the real and imaginary parts of the phase shift following the strategy of taking just one complex and energy dependent parameter at the innermost sampling point. This will generate a discretized energy dependence of Re $V(r_1, p_\alpha)$ and Im $V(r_1, p_\alpha)$, with $T_{\mathrm{LAB},\alpha} = 2p_{\mathrm{CM},\alpha}^2/M_N$ and $\alpha = 1, \ldots, N_{\mathrm{Dat}}$. In order to produce a smooth continuous curve we have also used the SAID solution, which we find produces worse fits than the set of discretized energies.

The dependence of the innermost real and imaginary parts is depicted in Fig. 8 while the remaining components are kept energy independent from the previous low energy fit. As we can see the behavior is quite different. While in the attractive core case both Re V_1 and Im V_1 exhibit a rather smooth energy dependence, the repulsive core scenario presents a rapid and sudden change already in the region where the inelasticity is
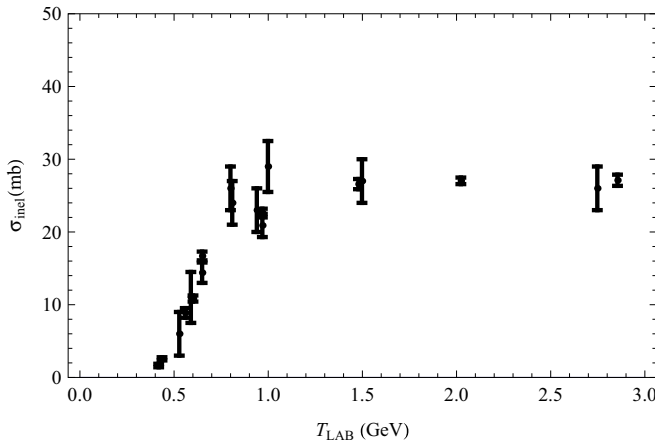
small. It is interesting to see what is the effect of switching off the inelastic contribution *without* refitting parameters. As we see in Fig. 9, the effect is dramatic in the standard repulsive core scenario and very mild in the attractive core case. Therefore, we can conclude that the inelastic contribution behaves truly as a perturbative effect in the structural core scenario.

VI. DISCUSSION AND OUTLOOK

A. The structural core and cluster models

Our finding for the repulsive branch echoes the result of Brown, 60 years ago [2]; namely, a rapid and nonadiabatic transition from a repulsive core to an extremely absorbing disk. The underlying and microscopic reason why this sudden change might happen has never been clarified, to our knowledge.

Unlike the repulsive branch, the attractive branch presents a deeply bound state at $E = -350$ MeV already at the lowest laboratory energy fits considered. This implies in particular that the zero energy wave function must have a node due to the oscillation theorem. In Fig. 2 (right) we show the zeroth energy wave function for both the attractive and repulsive branches in the 350 laboratory energy fit case. As we see, they both vanish at short distances and feature the difference between
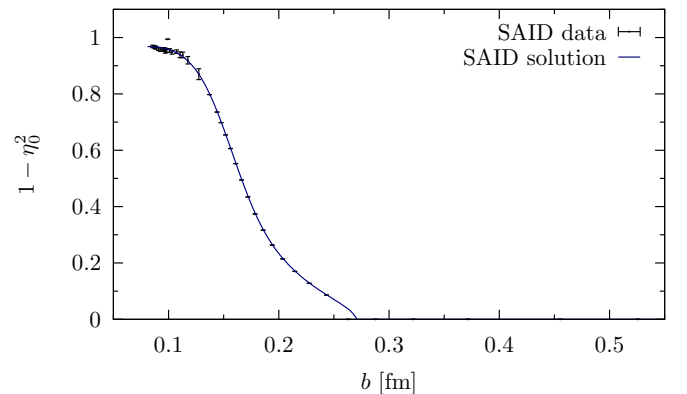

FIG. 6. Neutron-proton inelastic cross section as a function of laboratory energy [32]. The Δ and 2Δ resonance regions happen at $T_{\mathrm{LAB}} = 0.64$ GeV and $T_{\mathrm{LAB}} = 1.36$ GeV respectively.

FIG. 7. Neutron-proton inelasticity profile for the $^1S_0$ channel $1 - \eta_0(b)^2$ as a function of the impact parameter $b = (l + 1/2)/p$ for $l = 0$ from the SAID database.
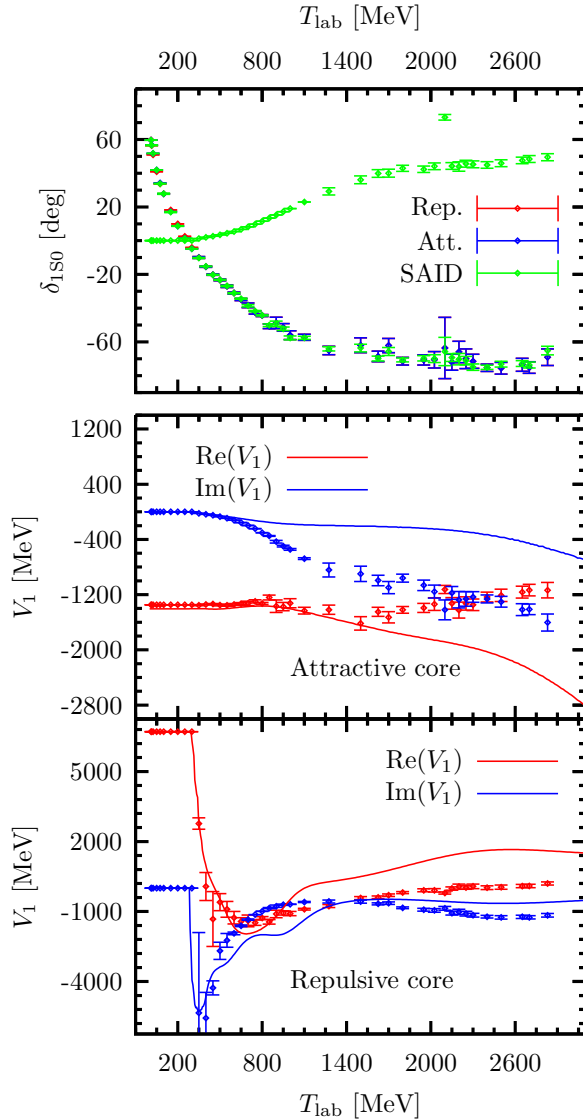
FIG. 8. Fit to the real and imaginary part of the $^1S_0$ np SAID phase-shift as a function of the laboratory energy up to 3 GeV for both the attractive and repulsive core cases (top panel). Energy dependence of the Re V_1 and Im V_1 values keeping the remaining parameters to the energy independent values for the attractive core (middle panel) and the repulsive core (bottom panel). Continuous lines represent using the SAID solution and discretized lines represent direct determination from scattering data.

the repulsive core, where the wave function vanishes below the core radius, and the structural core, where the wave function simply oscillates below the node. This pattern was already encountered in the OBE analysis and the main difference was taking an unnaturally large SU(3) violating $g_{\omega NN} \sim 20$ coupling constant or a natural one, $g_{\omega NN} = 3g_{\rho NN} \sim 10$ [27]. Here we confirm the trend when short distances are really probed by reproducing high energy scattering. The zero energy wave function pattern does not change much when the fitting energy is raised to 1 GeV, as can be seen in Fig. 3. In Fig. 10 we show the shape of the deeply bound state for two maximal fitting energies corresponding to fit $n = 5$ and $n = 10$ wells.
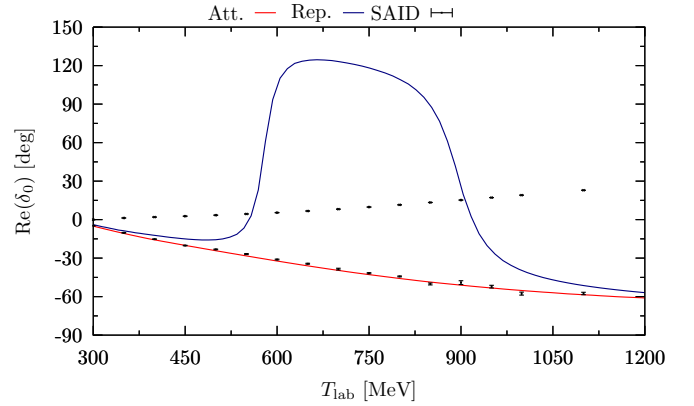

FIG. 9. Effect of switching off the imaginary part of the potential, Im $V_1 = 0$, keeping the remaining parameters in the $^1S_0$ np phase shift in the attractive and repulsive core scenarios.

Of course, this deeply bound state, while not influencing strongly the scattering, would provide a very negative contribution to the binding energy in finite nuclei by just placing pairs of protons and neutrons in $^1S_0$ channel with the relative spurious bound state wave function. While at first sight this may seem an unsurmountable problem for the structural core scenario, in what follows we argue why this spurious deeply bound state could and should indeed be removed from the potential, with no direct impact on the nuclear structure calculation.

The argument is based on old considerations on the structural core [7,20,21] and they are most easily and beautifully exemplified by the discussion of ^{8}Be made of two α clusters. Within a quark cluster model scheme for the nucleon, these nodes in the zero energy wave function are expected as a consequence of the Pauli principle of the constituent quarks, in which not all quarks belonging to different nucleons are simultaneously exchanged, and hence is a more general requirement than the Pauli principle for nucleons.

One should note that the exact location of the node is searched within the standard cluster Gaussian wave function approach because for these states the CM can be easily extracted. A nice interpretation of the phenomenon can be given within the Saito orthogonality condition model, which he analyzed thoroughly for two α clusters [85,86] (for comprehensive reviews see, e.g., [87,88]) and we remind here briefly adapted to the nucleon-nucleon situation. Due to the total antisymmetry of the wave function, the interaction term between clusters contains a direct (Hartree) and an exchange (Fock) term, where the quarks inside one nucleon are exchanged with the quarks in another nucleon. For a local quark-quark interaction the direct nucleon-nucleon term is also local whereas the exchange term is nonlocal, and this is a short-distance contribution which becomes negligible when the nucleons are at distances larger than their size. Thus, at large nonoverlapping distances the direct and local term survives and one can work within a Hartree approximation. Within a Hartree-Fock framework, Saito found that the Fock term had the effect of generating a node in the wave function when working in the Hartree approximation, i.e., when just the direct term is kept and the exchange term is ignored. Thus,
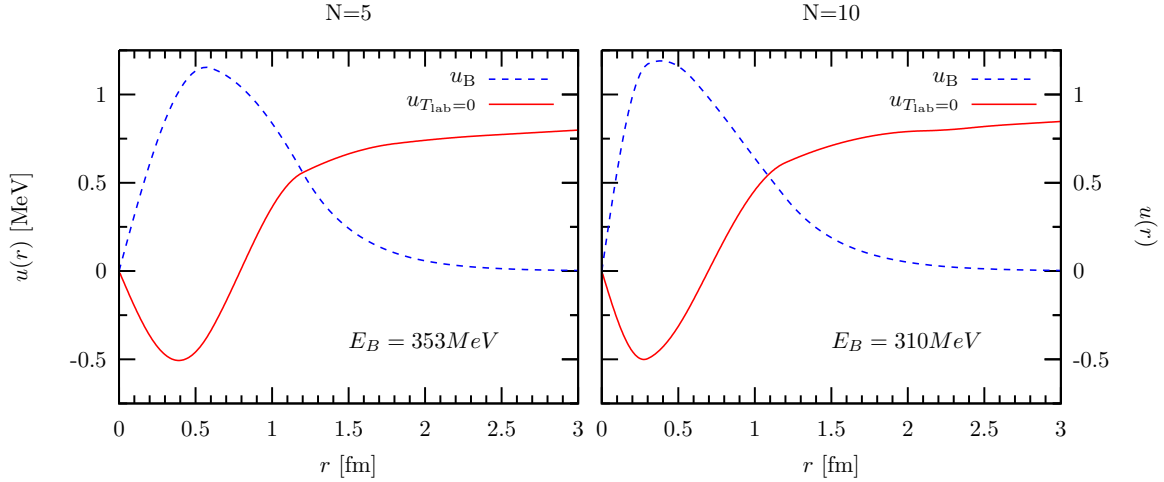
FIG. 10. Zero energy wave function and spurious Pauli-forbidden bound state when the fit is done with $n = 5$ (left) and $n = 10$ (right) square wells in the $^1S_0$ np phase shift in the attractive core scenario.

there is no direct nodeless zero energy wave function, since it is Pauli forbidden, and thus the corresponding deeply bound state which one finds in the Hartree approximation is spurious. The Fock term generates the extra node of the wave function and prevents the nodeless wave function.

Our coarse grained potential corresponds to just using the direct term. Therefore, the node we find in the zero energy wave function is just a manifestation of the composite character of the nucleons when they are handled as if they were elementary. These views have been advocated in several papers [22,23], motivating the series of Moscow potentials [24].

B. Extension to higher partial waves

The fact that coarse graining is working at these high energies in the case under study here with just S wave is encouraging. It would thus be quite interesting to extend the analysis to higher partial waves, and actually it should be possible to make a complete coarse grained PWA using the delta-shells regularization extending previous work at about the pion production threshold. Following the argument of a previous work [65] we may count the total number of parameters by setting the maximal angular momentum $l_{max} = p_{max}r_c$, and using $p_{max}\Delta r \sim 1$. On the other hand, for any $l \leqslant l_{max}$ we take $l(l + 1)/r_{min} = p_{max}^2$. Thus we get, using the 2×2 spin-isospin degeneracy factor corresponding to neutron and proton states with spins up and down,

$$N_{par} = 4 \sum_{l=0}^{l_{max}} \sum_n \theta\left(p^2 - \frac{l(l+1)}{r_n^2}\right) \sim 4\frac{1}{2}(p_{max}r_c)^2. \quad (28)$$

For the studied case here where $r_c = 3$ fm and $T_{LAB} = 3$ GeV, i.e., $p_{CM} = 1.26$ GeV, one gets $N_{par} \sim 700$, or equivalently $N_{par}^{pp} = N_{par}^{nn} \sim 175$ and $N_{par}^{pn} \sim 350$. These are large numbers of parameters, but not very different from the ones needed in the comprehensive most recent SAID np fit [43] based on a parametrization [37] with a total number of 147 parameters. It remains to be seen if these extra parameters might perhaps improve the quality of these fits since they describe 25 362

pp data with $\chi^2 = 48\,780.934$ and 13\,033 np data with $\chi^2 = 26\,261.000$.

C. Implications for nuclear physics

Fitting *NN* scattering data is not only a possible way to represent the data, but also the fitted potential is meant to be used in a nuclear structure calculation. While this seems most obvious, the well known complexities of the nuclear many-body problem require making a choice on the characteristic features of the potential itself. For instance, the mere concept of a repulsive core requires considering a local potential. This particular form is best suited for Monte Carlo type calculations and underlies the Argonne potentials saga [10–12]. Nonlocal or velocity dependent potentials do not exhibit the repulsive core so explicitly[5] and are usually handled by other techniques, such as the no-core shell model.

On the other hand, if we want to access to the short-distance region in finite nuclei by say, knock out processes (e, e', NN), we must fix the *NN* interaction going to high enough energies where both inelasticities and relativity ought to be important ingredients of the calculation. The resulting interaction, such as the one determined in the present paper, will thus become complex and energy dependent, and it is unclear at present how to use such an interaction in conventional nuclear structure calculations from an *ab initio* point of view where the main assumption is to take real and energy independent potentials. We hope to address these issues in the future.

D. Implications for hadronic physics

The fact that the coarse graining approach works for *NN* scattering in a regime where relativistic and inelastic effects become important suggests extending the method to other hadronic reactions under similar operating conditions, such

---

[5]It should be reminded that one can always perform a unitary phase-equivalent transformation from one form to another (see, e.g., [89] and references therein).

as $\pi\pi$ scattering up to $\sqrt{s} = 1.4$ GeV [90]. Within such a context the methods based in analyticity, dispersion relations and crossing are currently considered to be, besides QCD, the most rigorous framework (see, e.g., [91,92] and references therein). We stress that such an approach is based on the validity of the double spectral representation of the four-point function conjectured by Mandelstam. It is noteworthy that under this same assumption the optical potential of the form used in the present paper was derived many years ago [54,55]; analytic properties for $V(r,s)$ in the s variable in the form of a dispersion relation at *fixed* relative distance r were deduced. Due to their linear character, dispersion relations would be preserved under the coarse graining operation at the grid points for $V(r_i, s)$. In the present paper we have considered *NN* interaction taking both real and imaginary parts of the optical potential as independent variables. A much better procedure would be to constrain our fit to satisfy the fixed-r dispersion relations. This interesting study would require some sound assumptions on the interaction at high energies and is left for future research.

VII. CONCLUSIONS

We summarize our points. The repulsive nuclear core is a short-distance feature of the *NN* interaction which has been the paradigm in nuclear physics for many years. This allows us to not only to explain nuclear and neutron matter stability at sufficiently high densities, but also many realistic and successful *ab initio* calculations implement this repulsive core view, providing a compelling picture of short-range correlations, and even lattice QCD calculations seem to provide evidence on the repulsive core.

In this work we have tried to verify the paradigm by analyzing directly scattering data in a model independent way up to energies corresponding to a wavelength short enough to separate the well established core region from the rest of the potential. We have also critically analyzed recent evidence provided by lattice QCD calculations of *NN* potentials and seemingly supporting the repulsive core scenario. In light of the avoided crossing phenomenon triggered by multipion creation and disregarded in the lattice calculations, the repulsive core is just un upper bound of the true energy, and not a genuine feature of the *NN* interaction.

A coarse grained optical potential approach has been invoked, implementing a Wilsonian renormalization point of view. This is based in sampling the interaction with a complex potential at points separated by a sampling resolution corresponding to the minimal de Broglie wavelength, $\Delta r \sim 1/p_{\rm CM}$, for a given CM momentum, $p_{\rm CM}$. The number of sampling points is determined from the range of the region where the interaction is unknown. We assume, in agreement with previous low energy studies scanning the full database of $np + pp$ around the pion production threshold, that the interaction above $r_c = 3$ fm is given by the one-pion-exchange potential, and we sample the interaction at equidistant points separated by the resolution scale Δr.

Traditionally, the core region is estimated to be around $a_c \sim 0.5$ fm. This requires considering laboratory energies up to about 3 GeV, for which there exist comprehensive partial wave analyses. Since, the $^1S_0$ partial wave explores the shortest impact parameter $b \sim 1/(2p_{\rm CM})$, we have mainly restricted our analysis to this channel and have shown that the inelasticity is concentrated in a region below the resolution scale Δr. This amounts to treating the inelasticity interaction as pointlike and structureless. In the coarse grained setup, that means that we treat only the potential at the innermost sampling distance as complex and energy dependent. The remaining sampling points are kept real and energy independent. We have shown successful fits describing the real and imaginary parts of the $^1S_0$ phase shift up to 3 GeV laboratory energy. However, two conflicting scenarios emerge from these fits where the interaction at short distances becomes either strongly repulsive (the repulsive core) or strongly attractive (the structural core). Both scenarios have been considered in the past as alternative pictures of the *NN* interaction at short distances, and here we show explicitly how both arise from a similar way of sampling the interaction with a coarse grained potential. We corroborate the main difference between the two scenarios concerning the zero energy wave function, which vanishes below the core distance in the repulsive core case and has a node at about the core location but does not vanish below it in the structural core situation. Since these two scenarios are phase equivalent, we have analyzed in a comparative way some of their features, addressing the obvious question of which one is more realistic.

There is a remarkable and tangible difference between the short-distance repulsive-core and the structural-core scenarios, namely, the adiabaticity of the inelasticity. In the repulsive core case we get a rapid variation between a very strong short-distance repulsion and a very strong absorption. In contrast, in the structural core situation, the behavior is completely smooth, and the inelasticity couples in an adiabatic way as the energy is steadily increased.

On the other hand, while the repulsive core has no bound states, in agreement with experiment, the structural core presents a deeply bound state which might pose a problem for nuclear structure calculations. Cluster model studies have suggested that this deeply bound state is forbidden by the Pauli principle for the underlying quarks, and the node in the wave function is just a manifestation of the composite character of the nucleons. In fact, our way of solving the problem using an effective interaction at the hadronic level corresponds at the subnucleon level to considering just the direct Hartree term, whereas the exchange Fock term generates naturally the node of the relative wave function without the spurious bound state. The repulsive core branch presents a dramatic change from the core to a strongly absorbing potential, for which we are not aware of any microscopic explanation.

An interesting application is the study of nuclear processes where two particles are emitted at high relative momentum—which has implications for our understanding of short-distance correlations—since most studies in nuclear physics ignore the role of inelasticities when fixing the interaction at high energies. The fruitfulness of the coarse graining idea has been demonstrated recently in an efficient solution method of the Bethe-Goldstone equation and the presently obtained wave functions could be used to study the effects of inelasticity on short-range correlations; a task that has never been addressed and is left for future research.

Finally, the present study shows that the coarse graining idea works as expected at laboratory energies as high as 3 GeV, where the consideration of inelasticities is unavoidable, and suggests extending the present calculation to higher partial waves or other hadronic processes.

[1] R. Jastrow, Phys. Rev. **81**, 165 (1951).

[2] G. E. Brown, Phys. Rev. **111**, 1178 (1958).

[3] M. A. Preston and R. K. Bhaduri, *Structure of the Nucleus* (Elsevier, New York, 1975).

[4] T. Hamada and I. D. Johnston, Nucl. Phys. **34**, 382 (1962).

[5] R. V. Reid, Jr., Ann. Phys. (NY) **50**, 411 (1968).

[6] R. Tamagaki, Prog. Theor. Phys. **39**, 91 (1968).

[7] S. Otsuki, Prog. Theor. Phys. Suppl. **42**, 39 (1969).

[8] H. Bethe, *Nuclear Matter* (Academic, New York, 1970).

[9] R. Machleidt, Adv. Nucl. Phys. **19**, 189 (1989).

[10] I. E. Lagaris and V. R. Pandharipande, Nucl. Phys. A **359**, 331 (1981).

[11] R. B. Wiringa, R. A. Smith, and T. L. Ainsworth, Phys. Rev. C **29**, 1207 (1984).

[12] R. B. Wiringa, V. G. J. Stoks, and R. Schiavilla, Phys. Rev. C **51**, 38 (1995).

[13] S. C. Pieper and R. B. Wiringa, Annu. Rev. Nucl. Part. Sci. **51**, 53 (2001).

[14] J. Carlson *et al.*, Rev. Mod. Phys. **87**, 1067 (2015).

[15] Y. Nambu, Phys. Rev. **106**, 1366 (1957).

[16] R. A. Bryan and B. L. Scott, Phys. Rev. **135**, B434 (1964).

[17] R. Machleidt, Phys. Rev. C **63**, 024001 (2001).

[18] E. Oset, H. Toki, M. Mizobe, and T. T. Takahashi, Prog. Theor. Phys. **103**, 351 (2000).

[19] F. Gross, Phys. Rev. D **10**, 223 (1974).

[20] S. Otsuki, M. Yasuno, and R. Tamagaki, Prog. Theor. Phys. Suppl. **E65**, 578 (1965).

[21] R. Tamagaki, Rev. Mod. Phys. **39**, 629 (1967).

[22] V. G. Neudatchin *et al.*, Phys. Rev. C **11**, 128 (1975).

[23] V. G. Neudachin, Yu. F. Smirnov, and R. Tamagaki, Prog. Theor. Phys. **58**, 1072 (1977).

[24] V. I. Kukulin and V. N. Pomerantsev, Prog. Theor. Phys. **88**, 159 (1992).

[25] V. G. Neudatchin, N. P. Yudin, Y. L. Dorodnykh, and I. T. Obukhovsky, Phys. Rev. C **43**, 2499 (1991).

[26] V. I. Kukulin and M. N. Platonova, Yad. Fiz. **76**, 1549 (2013) [Phys. At. Nucl. **76**, 1465 (2013)].

[27] A. Calle Cordon and E. Ruiz Arriola, Phys. Rev. C **81**, 044002 (2010).

[28] S. Aoki (HAL QCD Collaboration), Prog. Part. Nucl. Phys. **66**, 687 (2011).

[29] S. Aoki, Eur. Phys. J. A **49**, 81 (2013).

[30] S. Aoki, J. Balog, and P. Weisz, Prog. Theor. Phys. **128**, 1269 (2012).

[31] L. D. Landau and E. M. Lifshits, *Quantum Mechanics Non-relativistic Theory* (translated from the Russian by J. B. Sykes and J. S. Bell), 2d ed. (Pergamon, Oxford, 1965).

[32] C. Lechanoine-LeLuc and F. Lehar, Rev. Mod. Phys. **65**, 47 (1993).

[33] J. Ball *et al.*, Eur. Phys. J. C **5**, 57 (1998).

[34] J. Bystricky, F. Lehar, and C. Lechanoine-LeLuc, Eur. Phys. J. C **4**, 607 (1998).

[35] J. Ball *et al.*, Nuovo Cimento A **111**, 13 (1998).

[36] R. A. Arndt, L. D. Roper, R. A. Bryan, R. B. Clark, B. J. VerWest, and P. Signell, Phys. Rev. D **28**, 97 (1983).

[37] R. A. Arndt, J. S. Hyslop, and L. D. Roper, Phys. Rev. D **35**, 128 (1987).

[38] R. A. Arndt, L. D. Roper, R. L. Workman, and M. W. McNaughton, Phys. Rev. D **45**, 3995 (1992).

[39] R. A. Arndt, C. H. Oh, I. I. Strakovsky, R. L. Workman, and F. Dohrmann, Phys. Rev. C **56**, 3005 (1997).

[40] R. A. Arndt, I. I. Strakovsky, and R. L. Workman, Phys. Rev. C **62**, 034005 (2000).

[41] R. A. Arndt, W. J. Briscoe, I. I. Strakovsky, and R. L. Workman, Phys. Rev. C **76**, 025209 (2007).

[42] Institute for Nuclear Studies, Data Analysis Center, N-N interaction, http://gwdac.phys.gwu.edu.

[43] R. L. Workman, W. J. Briscoe, and I. I. Strakovsky, Phys. Rev. C **94**, 065203 (2016).

[44] R. Shneor *et al.* (Jefferson Lab Hall A Collaboration), Phys. Rev. Lett. **99**, 072501 (2007).

[45] H. Feldmeier, W. Horiuchi, T. Neff, and Y. Suzuki, Phys. Rev. C **84**, 054003 (2011).

[46] M. Vanhalst, J. Ryckebusch, and W. Cosyn, Phys. Rev. C **86**, 044619 (2012).

[47] M. Alvioli, C. Ciofi Degli Atti, L. P. Kaptari, C. B. Mezzetti, and H. Morita, Int. J. Mod. Phys. E **22**, 1330021 (2013).

[48] R. B. Wiringa, R. Schiavilla, S. C. Pieper, and J. Carlson, Phys. Rev. C **89**, 024305 (2014).

[49] I. Ruiz Simo, R. Navarro Pérez, J. E. Amaro, and E. Ruiz Arriola, Phys. Rev. C **95**, 054003 (2017).

[50] K. O. Eyser, R. Machleidt, and W. Scobel, Eur. Phys. J. A **22**, 105 (2004).

[51] T. W. Allen, G. L. Payne, and W. N. Polyzou, Phys. Rev. C **62**, 054002 (2000).

[52] H. Feshbach, Ann. Phys. (NY) **5**, 357 (1958).

[53] H. Feshbach, Ann. Phys. (NY) **19**, 287 (1962); **281**, 519 (2000).

[54] J. M. Cornwall and M. A. Ruderman, Phys. Rev. **128**, 1474 (1962).

[55] R. Omnes, Phys. Rev. **137**, B653 (1965).

[56] T. Ueda, M. L. Nack, and A. E. S. Green, Phys. Rev. C **8**, 2061 (1973).

[57] S. G. Bondarenko *et al.*, Nucl. Phys. A **832**, 233 (2010).

[58] S. G. Bondarenko, V. V. Burov, and E. P. Rogochaya, Phys. Lett. B **705**, 264 (2011).

[59] E. Ruiz Arriola and W. Broniowski, Few-Body Syst. **57**, 485 (2016).

[60] E. Ruiz Arriola and W. Broniowski, Phys. Rev. D **95**, 074030 (2017).

[61] D. R. Entem, E. Ruiz Arriola, M. Pavon Valderrama, and R. Machleidt, Phys. Rev. C **77**, 044006 (2008).

[62] R. Navarro Perez, J. E. Amaro, and E. Ruiz Arriola, Prog. Part. Nucl. Phys. **67**, 359 (2012).

[63] R. Navarro Perez, J. E. Amaro, and E. Ruiz Arriola, Few-Body Syst. **54**, 1487 (2013).

[64] R. Navarro Pérez, J. E. Amaro, and E. Ruiz Arriola, Phys. Rev. C **88**, 064002 (2013); **91**, 029901(E) (2015).

[65] R. Navarro Perez, J. E. Amaro, and E. Ruiz Arriola, Few-Body Syst. **55**, 983 (2014).

[66] R. Navarro Pérez, J. E. Amaro, and E. Ruiz Arriola, Phys. Lett. B **724**, 138 (2013).

[67] K. Chadan and P. Sabatier, *Inverse Problems in Quantum Scattering Theory* (Springer-Verlag, Berlin, 1989).

[68] H. Leeb, H. Fiedeldey, and R. Lipperheide, Phys. Rev. C **32**, 1223 (1985).

[69] N. A. Khokhlov and V. A. Knyr, arXiv:nucl-th/0410092.

[70] H. V. von Geramb, K. A. Amos, H. Labes, and M. Sander, Phys. Rev. C **58**, 1948 (1998).

[71] A. Funk, H. V. von Geramb, and K. A. Amos, Phys. Rev. C **64**, 054003 (2001).

[72] V. A. Knyr, V. G. Neudachin, and N. A. Khokhlov, Yad. Fiz. **69**, 2079 (2006) [Phys. At. Nucl. **69**, 2034 (2006)].

[73] N. A. Khokhlov and V. A. Knyr, Phys. Rev. C **73**, 024004 (2006).

[74] K. A. Wendt, R. J. Furnstahl, and S. Ramanan, Phys. Rev. C **86**, 014003 (2012).

[75] J. B. Aviles, Phys. Rev. C **6**, 1467 (1972).

[76] S. Albeverio *et al.*, J. Math. Phys. **54**, 052103 (2013).

[77] R. Navarro Pérez, J. E. Amaro, and E. Ruiz Arriola, Phys. Rev. C **95**, 064001 (2017).

[78] A. Sibirtsev *et al.*, Eur. Phys. J. A **45**, 357 (2010).

[79] W. P. Ford and J. W. Van Orden, Phys. Rev. C **87**, 014004 (2013).

[80] R. Navarro Perez, J. E. Amaro, and E. Ruiz Arriola, Phys. Rev. C **89**, 064006 (2014).

[81] E. Oset and L. L. Salcedo, J. Comput. Phys. **57**, 361 (1985).

[82] R. Navarro Pérez, E. Ruiz Arriola, and J. Ruiz de Elvira, Phys. Rev. D **91**, 074014 (2015).

[83] R. Navarro Pérez, J. E. Amaro, and E. Ruiz Arriola, Phys. Lett. B **738**, 155 (2014).

[84] B. A. Ryan *et al.*, Phys. Rev. D **3**, 1 (1971).

[85] S. Saito, Prog. Theor. Phys. **41**, 705 (1969).

[86] S. Saito, Prog. Theor. Phys. Suppl. **62**, 11 (1977).

[87] Y. C. Tang, M. LeMere, and D. Thompsom, Phys. Rep. **47**, 167 (1978).

[88] H. Friedrich, Phys. Rep. **74**, 209 (1981).

[89] T. Neff, H. Feldmeier, and W. Horiuchi, Phys. Rev. C **92**, 024003 (2015).

[90] J. Ruiz de Elvira and E. Ruiz Arriola (unpublished).

[91] B. Ananthanarayan *et al.*, Phys. Rep. **353**, 207 (2001).

[92] R. Garcia-Martin, R. Kaminski, J. R. Pelaez, J. Ruiz de Elvira, and F. J. Yndurain, Phys. Rev. D **83**, 074004 (2011).